Effect of Solidification Behaviors of Mold Fluxes on the Heat Flux in Thin Slab Casting Mold

Jung Wook Cho, Seong-Yeon Kim, Suk Chun Moon* and Hiroyuki Shibata**

Kwangyang Iron & Steelmaking Research Group
Pohang Iron & Steel Co., Ltd.
699, Kumho-Dong, Kwangyang-Shi, Cheonnam, 545-090, Korea
E-mail pc808650@posco.co.kr
*Minimill Dept.
Pohang Iron & Steel Co., Ltd.
699, Kumho-Dong, Kwangyang-Shi, Cheonnam, 545-090, Korea
**Institute for Advanced Material Processing
Tohoku University
2-1-1 Katahira, Aobaku, Sendai 980-77 Japan

ABSTRACT

Crystallization of molten mold flux film has been observed with a confocal scanning laser microscope (CSLM). The observation has indicated that mold flux of higher basicity starts crystallizing directly in liquid phase at higher temperature, and shows faster growth than that of lower basicity. Cross section of solidified fluxes shows that the shrinkage due to the crystallization is more for higher basicity flux than lower one. This implies that thermal resistance at mold/mold flux film interface arises from the solidification and crystallization of the flux film. Referring to the results, contraction of commercial mold fluxes during solidification has been investigated using a stainless steel mold. The observed contraction amount has been compared with the heat flux from the plant caster. The larger contraction results in smaller mold heat flux, which gives a conclusion that the larger solidification contraction will cause larger interfacial thermal resistance in mold.

1. INTRODUCTION

The thin slab casting processes have been applied worldwide for the last few years. High casting speed is essential in these processes because the cast slabs must be transferred to hot rolling mill continuously. However, increased heat flux in mold at the higher casting speeds tends to cause more longitudinal cracks on the slab surface especially for peritectic medium carbon steel the solidifying shell of which grows irregularly due to enhanced shrinkage on δ to γ transformation. Therefore, it is desirable to suppress the mold heat flux even at high casting speed to maintain sound surface.

Basic mold fluxes with high crystallizing temperatures are known to be effective to reduce the occurrence of surface cracks by decreasing the heat flux. Recently, some researchers [1-4] reported that the reason for the decrease in mold heat flux is mainly due to the large interfacial thermal resistance between mold flux film and mold. However, the controlling factor on the interfacial resistance has not been made clear yet.

In the present paper, the crystallization of mold fluxes was investigated using a confocal scanning laser microscope to clarify the origin of the interfacial thermal resistance. Moreover, effect of solidification behaviors, contraction and surface roughness during crystallization, on the mold heat flux in thin slab caster was investigated in consideration of interfacial thermal resistance.

2. PREVIOUS WORK

In continuous casting, heat from solidifying shell is transferred by conduction and radiation to mold. If there are no interactions between processes, the overall thermal resistance can be expressed by conductive, radiative and interfacial components as shown in Fig.1. Conductive and radiative thermal resistance can be calculated from measured thermal conductivity and absorption coefficient, respectively, for both crystalline and molten layer of mold flux film.

2-1. Conductivity of mold flux

Reliable conductivity data for molten mold fluxes has been obtained by Shibata and Ohta [5,6], who developed a differential three layer laser flash method. In addition, they distinguished the effect of radiation from measured result, and reported that thermal conductivities of fluxes exist between 1.2~1.4 W/(mK) which agree well with the extrapolated value of solid glass. These values are a little smaller than that of crystalline fluxes, 1.4~1.8W/(mK), mainly because the movement of phonons will be restricted by the randomness of the structure of molten mold flux. Little difference was found between the commercial mold fluxes for low carbon and for medium carbon steels mainly because the basicity, two fluxes are not much different.

2-2. Radiative property of mold flux

Kusabiraki et al. [7] measured the transmittance of various oxides, and reported that there are not remarkable differences between solid glassy and molten phase. Thus, it would result little error in calculating heat flux by using the absorption coefficient of solid glass for radiative heat transfer across molten layer of mold flux film. Absorption coefficient and extinction coefficient of commercial mold fluxes have been determined to evaluate the radiative heat transfer through infiltrated film of these fluxes in continuous casting mold by Cho et al. [8]. The absorption coefficient is found to be less than $1000m^{-1}$ for glassy films whereas the extinction coefficient is ca. $3000\sim30000m^{-1}$ for crystalline ones in their study. Also, the difference in the chemical composition of commercial mold fluxes has little systematic influence on the absorption behavior in the visible and infrared range, and hence on the behavior of radiative heat transfer across the flux film.

2-3. Interfacial thermal resistance between mold flux film and mold

Ohmiya et al. [9] carried out a pioneering measurement of interfacial thermal resistance using miniature scale mold. They found that contact resistance occurs when the substance between copper mold and steel plate is a solid, and reported the values of $1.3x10^{-4}m^2K/W$ for solid paraffin, and $3.6x10^{-4}m^2K/W$ for solid CuCl+KCl. Yamauchi et al. [10] carried out similar experiment for commercial mold flux film, and reported the presence of interfacial thermal resistance of ca. $4\sim8x10^{-4}m^2K/W$. Because the mold side surface temperature of the mold flux film could not be measured directly in these observations, interfacial thermal resistances were derived indirectly [10] by assuming that the effective thermal conductivity is independent of overall flux film thickness.

However, the reliability of this assumption is subject to question by Cho et al. [1]. They reported that interfacial thermal resistances increases with increasing flux film thickness, as

shown in Fig.2, in contrast to previous observation by others who assumed that the interfacial thermal resistance is constant for different flux film thickness. The interfacial thermal resistances is found to be more than 50% of overall thermal resistance for the heat transfer at the near meniscus position in mold. Observed low heat flux for the mold flux with high crystallization temperature is then attributed to high interfacial thermal resistance.

3. IN-SITU OBSERVATION OF CRYSTALLIZATION OF MOLD FLUX

In the previous studied, it has been found that the interfacial thermal resistance between copper mold and crystallized mold flux film, which arises from the crystallization of mold flux, plays a most important role in the heat transfer in casting mold. Therefore, it is highly desirable to clarify the effects of physiochemical properties of mold flux on the crystallizing phenomena. In this paper, an in-situ observation of the crystallization of commercial mold flux melt on cooling will be described. Observation was carried out using a confocal scanning laser microscope (CSLM) with infrared image furnace. Origin of interfacial thermal resistance will be discussed with the results of in-situ observation.

3-1. Experiment of CSLM observation

Mold fluxes for high speed casting of low carbon steel (LC2) and medium carbon steel (MC2) were selected same as shown in previous studies of author [1,2,8]. These mold fluxes, after burning off the skeleton materials, were melted in a platinum crucible, held for 10 min at 1673K and quenched on a copper plate before experiment. The chemical compositions of applied mold fluxes with other physical properties are shown in Table 1.

Crystallization of mold fluxes was observed using a CSLM with infrared image furnace. The mold fluxes of 0.07~0.12g were mounted in a platinum crucible of 5mm outer diameter and 5mm height. During experiments, the confocal images including the information on time and temperature were recorded on videotape and monitored simultaneously on a CRT. More detailed description about the CSLM with an infrared image furnace has been given by Chikama et al. [11].

Crystallizing temperatures for present mold fluxes were also measured using DTA on cooling from 1673K at 10K/min. Observed crystallizing temperatures were compared with those from the observation of CSLM. Morphology and chemical composition of crystalline was identified and determined by using an energy disperse spectrometer (EDS) attached to a scanning electron microscope (SEM) after CSLM observation.

3-2. Observation of crystallization

The molten mold fluxes are almost transparent for the incident beam wavelength in the range of ca. 0.5-2.5μm [12]. As the wavelength of He-Ne laser used in CSLM is 0.633 μm, it is possible to observe the bottom of platinum crucible through molten mold flux as shown in Fig. 3(a). The grain boundaries of platinum and voids formed between the bottom of the mold flux melt and crucible are observed as shown in Fig. 3(a). When a mold flux crystallizes, image of the bottom of the crucible turns to be dark as crystals grow as shown in Fig. 3(a) and (b) due to much larger absorption coefficient [8] of the crystalline phases and grain boundaries. The crystallization of mold flux initiates near the surface, as can be seen in the similar shape between dark region in Fig. 3(b) and growing crystalline in Fig. 3(c). The crystalline mold flux does not show a good contrast with molten mold flux as shown in Fig. 3(c) because both phases have small difference in reflectivity.

3-3. Crystallizing behavior of mold flux

The crystallization of LC2 mold flux was observed at a cooling rate of 10K/min from 1573K as shown in Fig. 4. The primary crystallization initiated at 1284K, and granular crystalline phase could be observed on the surface in Fig. 4(a). These crystals grew slowly as shown in Fig. 4(a) to (c), and hence most part of mold flux remained as glassy. A secondary crystallization occurred in remained glassy mold flux at 972K. The primary crystalline phase is identified as Cuspidine, $3CaO2SiO_2CaF_2$, and the secondary as Nepherine, $Na_2OAl_2O_32SiO_2$ by EDS analysis.

The MC2 mold flux also crystallized twice, at 1393K and 877K, with a cooling rate of 10K/min from 1573K to 1273K, and 50K/min from 1273K. Interference can be seen on the surface of growing crystals in the primary crystallization because the crystals were covered with remained glassy phase as shown in Fig. 5. The primary crystals of MC2 grew much faster than those of LC2, and this growth is rather dentritic than globular as shown in Fig. 5. Therefore, the amount of remained glassy phase for MC2 is smaller than that for LC2. The primary crystalline phase of MC2 is also found to be Cuspidine. However, the secondary one has not been clarified yet.

Observed crystallizing temperatures as shown in Figs. 4 and 5 show good correlation to the obtained peak temperatures determined by DTA at a cooling rate of 10K/min from 1573K as listed in Table. 2.

3-4. Morphology of crystalline phase

The cross section of crystalline mold fluxes after CSLM observation were investigated by scanning electron microscopy. The granular crystals of LC2 are much larger than those of dendritic MC2 as shown in Figs. 6 and 7. The main phase of both mold fluxes, which is white region in Figs. 6 and 7, are identified as Cuspidine by EDS analysis. The dark region of LC2 in Fig. 6(b) consists of secondary Nepherine and remained glassy, while no other crystalline phase can be seen in MC2. Dendritic growth can also be seen at the boundaries of granular Cuspidine crystals. However, higher cooling speed would be needed to develop more distinct dendritic microstructure.

It should be noted that substantial shrinkage occurred in MC2, which is believed to come from faster growth rate of primary crystalline for MC2 than that of LC2. This agrees with and explains larger interfacial thermal resistance of MC2 mold flux than that for LC2. Thus, this difference in shrinkage due to the crystallization behavior between the two mold fluxes is concluded responsible for the slow cooling of steel slabs in continuous casting mold at the initial stage of solidification when basic mold flux high in crystallizing temperature is applied.

4. EFFECT OF SOLIDIFICATION CONTRACTION ON THE HEAT FLUX

Through the observation of crystallizing behavior of mold fluxes, it has been found that the crystallizing behavior of mold fluxes is considerably affected by the chemical composition. It is supposed that crystal growth speed and volumetric contraction during solidification will cause the difference in interfacial thermal resistance. In this part, volumetric contraction of commercial mold fluxes during solidification was investigated by pouring melts into stainless steel mold to clarify the solidification behavior of mold fluxes.

4-1. Experiment of solidification

Chemical composition and physical properties of mold fluxes in this study are shown in Table 3. These mold fluxes were melted in a graphite crucible, held for 20 min at 1623K and cooled in a stainless steel mold at 623K.

The schematic of mold and specimen is shown in Fig.8. One hundred gram of molten mold flux was poured into the mold, of which the internal dimension was 60mm width, 30mm length and 40mm height. The cooling rates at 1273K were approximately 2.5K/sec at the center and 12K/sec at the bottom of the specimen. As illustrated in Fig.8, the side and bottom of the specimen that contacted with mold plate usually remained glassy state, while the top and center were crystallized. Amount of contraction and surface roughness were measured on the top of the specimen after cooling, as shown in Fig.8. These solidification properties of mold flux were compared with heat flux of thin slab caster at Kwangyang Works.

4-2. Relationship between solidification properties and heat flux

Crystalline phase is dendritic microstructure at the center of the specimen, and it gradually changes into equiaxed structure moving to top, as shown in Fig.8. Because the thickness of crystalline in middle of specimen is larger than that of edge, it is believed that the depression on the top surface arises from the volumetric contraction when the glassy mold flux is crystallized. All the crystalline in Fig.8 have been found as Cuspidine by EDS observation.

When the mold flux that has larger solidification contraction was applied, heat flux generally decreased as shown in Fig.9. This implies that the larger solidification contraction will cause larger interfacial thermal resistance in mold.

Some of previous researchers reported that larger surface roughness of crystalline results larger interfacial thermal resistance [4]. However, the mold fluxes which are believed to have larger interfacial thermal resistance (Flux C, D) show slightly smaller surface roughness of crystalline than Flux A and B, as shown in Fig.10. From the relation between surface morphology and roughness profile in Fig.11, it is found that the surface roughness was affected not only by the crystallizing tendency but also by the grain size of surface crystalline. Because the grain size of Cuspidine is prone to decrease at the highly basic mold flux system due to increased embryos, as can be seen in Figs. 6 and 7, it is believed that the surface roughness does not give a meaningful effect on interfacial thermal resistance. It should be emphasized, therefore, that mold flux which has large solidification contraction should be developed for slow cooling in the continuous casting mold.

5. CONCLUSIONS

Crystallization of mold fluxes were observed in-situ using a confocal scanning laser microscope with an infrared image furnace to clarify the origin of interfacial thermal resistance in mold. Also, the effects of solidification contraction and surface roughness during crystallization on mold heat flux in thin slab caster were investigated. The major results obtained can be summarized as follows:

(1) The crystallizing temperatures observed in confocal scanning laser microscope (CSLM) agree well with those from differential thermal analysis (DTA). It is found that the combination of DTA and in-situ observation using CSLM is an effective method to understand the crystallization behavior of mold flux.

(2) The cross section of the mold flux of higher basicity shows larger shrinkage during crystallization than that of lower one mainly because of much higher growth rate of primary

Cuspidine. This difference in shrinkage will cause larger interfacial thermal resistance when high basicity mold flux is infiltrated between copper mold and solidified steel shell.

(3) The larger contraction during cooling in stainless mold results in smaller mold heat flux in thin slab caster, which implies that the larger solidification contraction will cause larger interfacial thermal resistance in mold.

REFFERENCES

1) J. W. Cho, H. Shibata, T. Emi and M. Suzuki, "Thermal Resistance at the Interface between Mold Flux Film and Mold for Continuous Casting of Steels", ISIJ Int., **38** (1998), 440
2) J. W. Cho, H. Shibata, T. Emi and M. Suzuki, "Heat Transfer across Mold Flux Film in Mold during Initial Solidification in Continuous Casting of Steel", ISIJ Int., **38** (1998), 844
3) K. Watanabe, M. Suzuki, K. Murakami, H. Kondo, A. Miyamoto and T. Shiomi, "The Effect of Crystallization of Mold Powder on the Heat Transfer in Continuous Casting Mold", Testu-to-Hagane, **83** (1997), 115
4) K. Tsutsumi, T. Nagasaka and M. Hino, "Surface Roughness of Solidified Mold Flux in Continuous Casting Process", ISIJ Int., **39** (1999), 1150
5) H. Shibata, K. Kondo, M. Suzuki, and T. Emi, "Thermal Resistance between Solidifying Steel Shell and Continuous Casting Mold with Intervening Flux Film", ISIJ Int., **36** (1996), supplement, S179
6) H. Ohta, M. Msuda, K. Watanabe, K. Nakajima, H. Shibata and Y. Waseda, "Determination of Thermal Diffusivities of Continuous Casting Powders for Steel by Precisely Excluding the Contribution of Radiative Component at High Temperature", Testu-to-Hagane, **80** (1994), 463
7) K. Kusabiraki and Y. Shiraishi, "Infrared Emission Spectra of Molten Alkaline Metal Silicates", J. Japan Inst. Metals, **45** (1981), 250
8) J. W. Cho, T. Emi, H. Shibata and M. Suzuki, "Radiative Heat Transfer through Mold Flux Film during Initial Solidification in Continuous Casting of Steel", ISIJ Int., **38** (1998), 268
9) S. Ohmiya, K. H. Tacke and K. Schwerdtfeger, "Heat Transfer through Layers of Casting Fluxes", Ironmaking and Steelmaking, **10** (1983), 24
10) A. Yamauchi, K. Sorimachi, T. Sakuraya and T. Fujii, "Heat Transfer between Mold and Slab through Mold Flux Film in Continuous Casting of Steel", ISIJ Int., **33** (1993), 140
11) H. Chikama, H. Shibata, T. Emi and M. Suzuki, "In-situ Real Time Observation of Planar to Cellular and Cellular to Dendritic Transition of Crystals Growing in Fe-C Alloy Metals," Mater. Trans. JIM, **37** (1996), 620
12) M. Susa, K. C. Mills, M. J. Richardson, R. Taylor and D. Stewart, "Thermal Properties of Slag Films Taken from Continuous Casting Mould", Ironmaking and Steelmaking, **21** (1994), 279

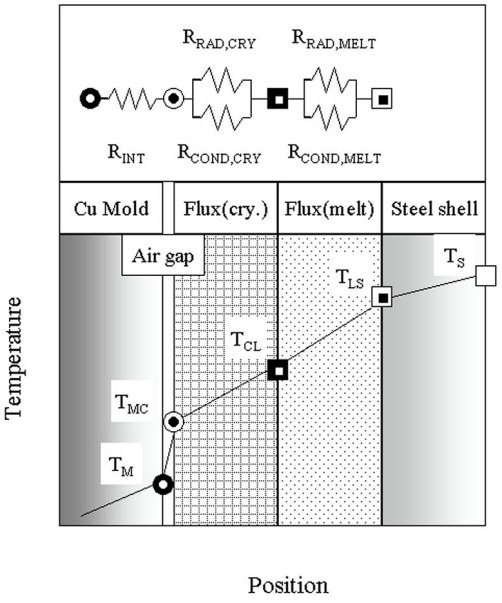

Fig.1. Temperature distribution across mold flux film consisting of crystalline and molten layers

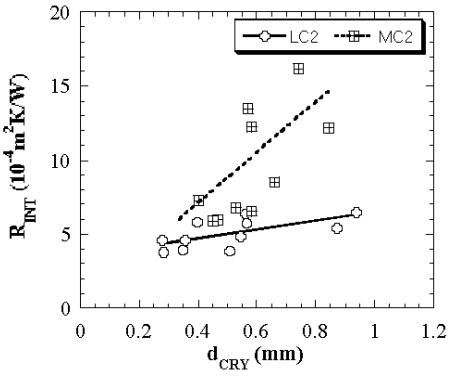

Fig.2 Change of observed interfacial thermal resistance with thickness of crystalline layer of mold flux film

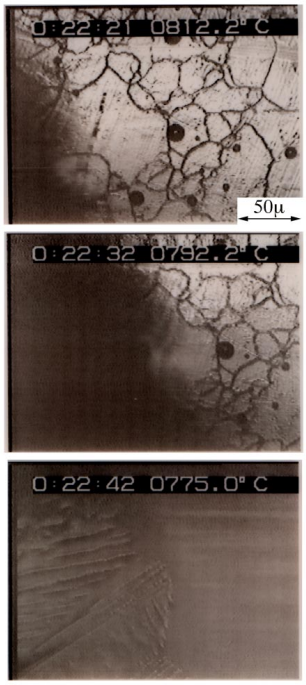

(a) initiation of crystallization

(b) growth of primary crystalline phase

(c) observed crystal phase on mold flux surface

Fig.3 Initiation of crystallization of LC2 mold flux with cooling rate of 100K/min

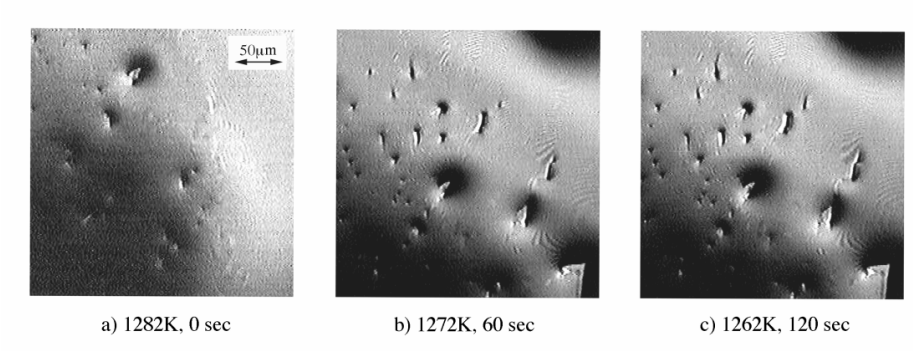

a) 1282K, 0 sec b) 1272K, 60 sec c) 1262K, 120 sec

Fig.4 Growth of primaty crystalline phase of LC2 mold flux

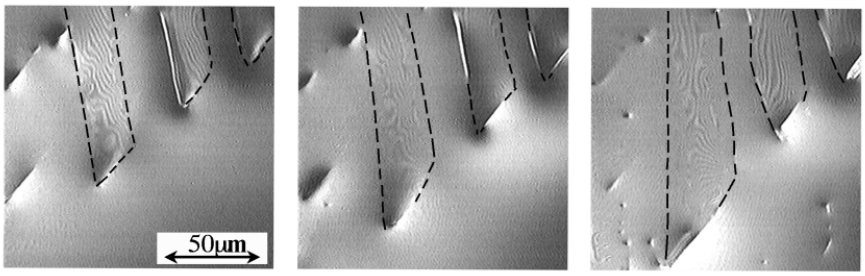

a) 1392K, 0 sec b) 1391K, 2 sec c) 1376K, 100 sec

Fig.5 Growth of primaty crystalline phase of MC2 mold flux

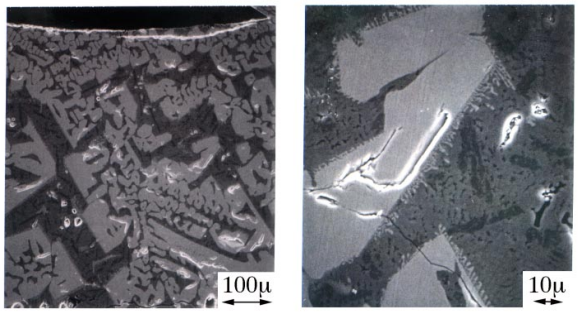

Fig.6 SEM micrographs of cross section of crystalline LC2 mold flux after CSLM observation

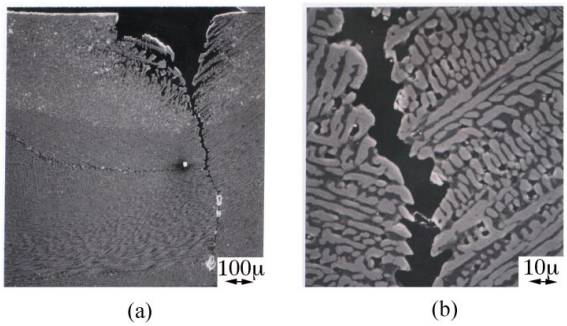

Fig.7 SEM micrographs of cross section of crystalline MC2 mold flux after CSLM observation

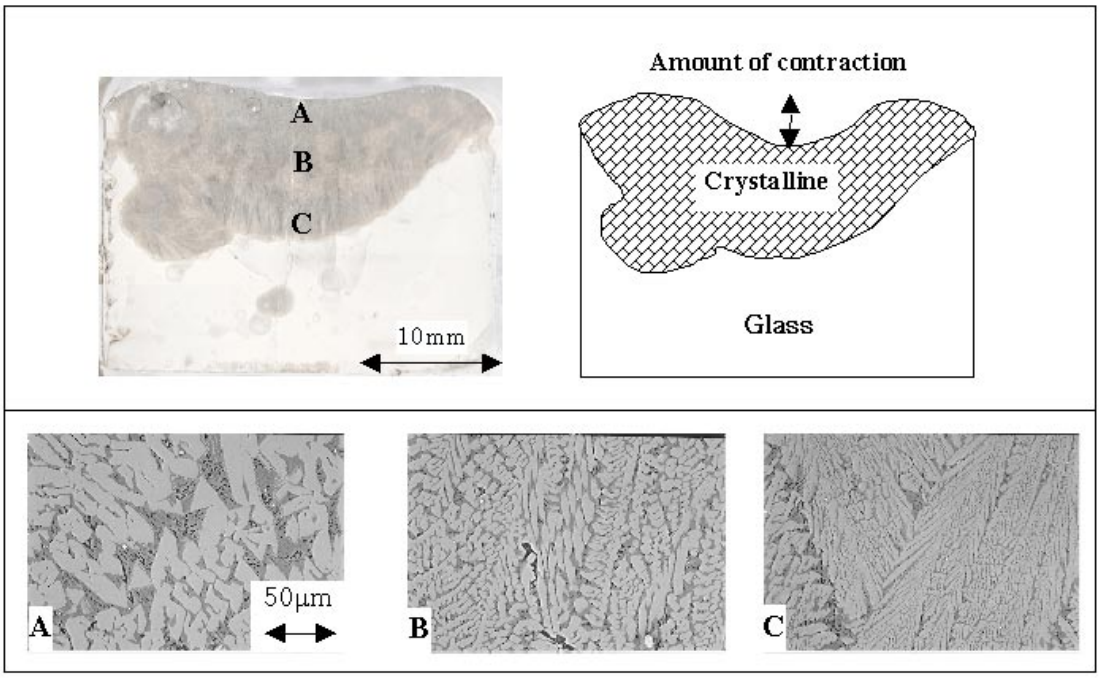

Fig.8 Typical microstructure of the cross section of specimen

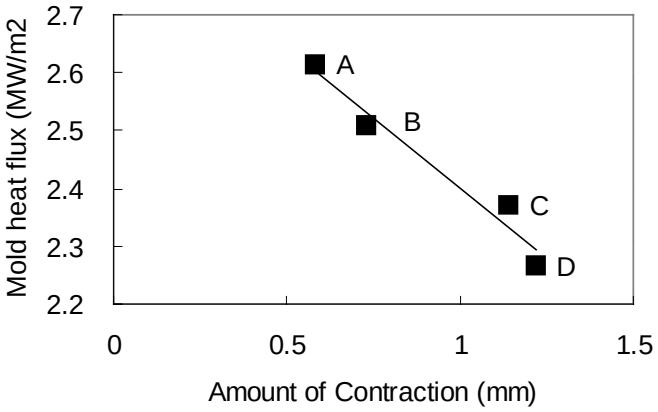

Fig.9 Relationship between solidification contraction and mold heat flux

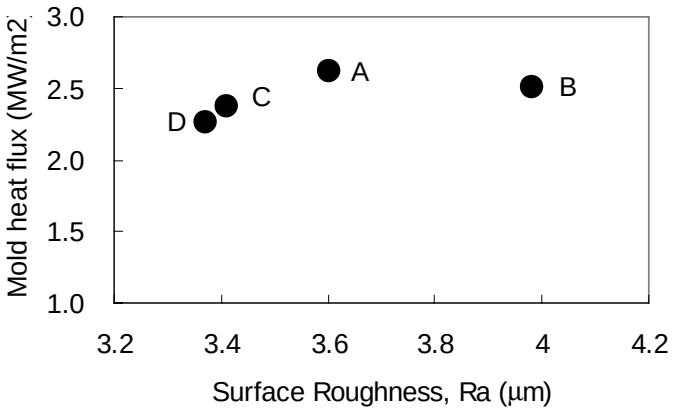

Fig.10 Relationship between surface roughness of crystalline and mold heat flux

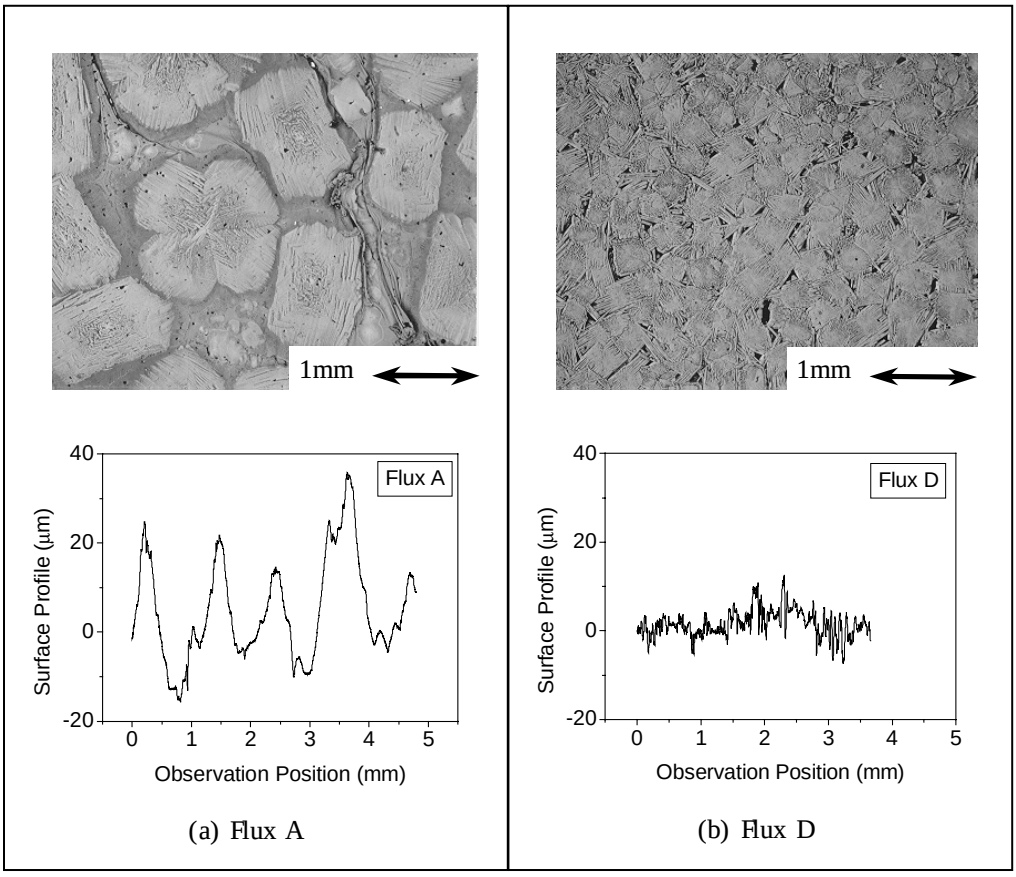

(a) Flux A (b) Flux D

Fig.11 SEM micrographs on the top surface with surface profile

Table 1 Chemical composition (in mass %) and physical properties of mold fluxes used

Mold flux	LC2	MC2
Steel grade applied	low carbon	medium carbon
SiO_2	35.0	31.8
CaO	33.8	44.8
Al_2O_3	6.4	3.7
Fe_2O_3	0.7	0.4
Na_2O	11.2	7.3
MgO	2.3	1.9
MnO	0.1	0.1
TiO_2	0.1	0.1
K_2O	0.5	0.3
Li_2O	4.6	3.9
F	8.4	9.9
CaO/SiO_2	0.96	1.41
Viscosity (Poise at 1573K)	0.9	0.5
Crystallization temperature(K)	1313	1436

Table 2 Comparison of observed crystallizing temperatures by CSLM with those measured by DTA.

LC2		MC2	
DTA	CLSM	DTA	CLSM
1302K	1284K*	1415K	1393K*
1012K	976K**	1058K	Not observed
		960K	877K***

* Cuspidine: $3CaO2SiO_2CaF_2$

** Nepherine: $Na_2OAl_2O_32SiO_2$

*** undefined: $Na_2OAl_2O_3xMgOySiO_2$, where x: 1~3, y:2~6

Table 3 Chemical composition and physical properties of mold fluxed used

Mold flux	A	B	C	D
CaO/SiO_2	1.00	1.29	1.32	1.35
F	7.1	10.2	9.0	9.0
Viscosity (Poise at 1573K)	0.72	0.60	0.53	0.55
Steel grade applied	low carbon medium carbon		medium carbon	